Lifespan dynamics of cluster conformations in stationary regimes in granular materials

Na Deng
Grenoble Alps University, INRAE, UR ETNA, 2 rue de la Papeterie-BP 76, 38402 St-Martin-d'Hères, France

Antoine Wautier*
Aix-Marseille University, INRAE, UMR RECOVER, 3275 Rte Cézanne, CS 40061, 13182 Aix-en-Provence Cedex 5, France

Antoinette Tordesillas
School of Mathematics and Statistics, The University of Melbourne, Melbourne, Victoria, 3010, Australia

Yannick Thiery
BRGM (French Geological Survey), Risk and Prevention Division, 3 Av. Claude Guillemin, 45100, Orléans, France

Zhen-Yu Yin
Department of Civil and Environmental Engineering, The Hong Kong Polytechnic University, Hong Kong, China

Pierre-Yves Hicher
Research Institute in Civil Engineering and Mechanics (GeM), UMR CNRS 6183, Ecole Centrale de Nantes, 1 Rue de la Noë, 44300, Nantes, France

François Nicot
Grenoble Alps University, INRAE, UR ETNA, 2 rue de la Papeterie-BP 76, 38402 St-Martin-d'Hères, France and Université Savoie Mont Blanc, Laboratoire EDYTEM, UMR 5204, 5 bd. de la Mer Caspienne, 73376 Le Bourget-du-Lac, France

(Received 19 July 2021; accepted 17 December 2021; published 7 January 2022)

We examine stationary regimes in granular materials from a dynamical systems theory perspective. The aim is to enrich the classical view of the critical state regime in granular materials, and more broadly, to improve the fundamental understanding of the underlying mesoscale mechanisms responsible for macroscopic stationary states in complex systems. This study is based on a series of discrete element method simulations, in which two-dimensional assemblies of nonuniformly sized circular particles are subjected to biaxial compression under constant lateral confining pressure. The lifespan and life expectancy of specific cluster conformations, comprising particles in force chains and grain loops, are tracked and quantified. Results suggest that these conformational clusters reorganize at similar rates in the critical state regime, depending on strain magnitudes and confining pressure levels. We quantified this rate of reorganization and found that the material memory rapidly fades, with an entirely new generation of force chains and grain loops replacing the old within a few percent strain.

DOI: 10.1103/PhysRevE.105.014902

I. INTRODUCTION

Stationary regimes exist in a great variety of complex systems, which comprise large numbers of interacting units [1–3]. At the macroscopic scale, such systems may be characterized by statistical descriptors that remain constant over time, while underlying local scale interactions between components continually change. In the case of granular materials, where the internal degrees of freedom are large, a multitude of *conformations* (arrangements of particle structures) and *conformational transitions* [4–12] exist for which the macroscopic stress and porosity remain constant under continuous shearing. Such macroscopic states, called critical states (CSs) in the geomechanics community, form the focus of critical state theory (CST) [13–15], which stands as a cornerstone of constitutive theory for granular materials. Constitutive laws built on CST are, however, phenomenological and cannot account for the underlying conformational transitions which are responsible for the emergence of critical states. In this respect, only multiscale models may capture the underlying microscale detailed balance. But, many aspects of these transitions remain poorly understood, and no multiscale model exists in which (i) the minimal set of conformational transitions responsible for the emergence of critical states, and (ii) the rate of reorganization are embedded. Indeed, novel structures, transitions, and regimes are still being uncovered in granular materials under shear, mostly thanks to the use

*Corresponding author: antoine.wautier@inrae.fr

of discrete element modeling (DEM), as well as advanced experimental equipment [16].

One line of advance, which is pursued in this study, is to adopt a dynamical systems theory (DST) approach to improve the fundamental understanding of the critical state by focusing on conformational transitions from the perspective of two important classes of mesostructures, namely force chains and grain loops [4–6] (see the definitions in Appendix B). Here we similarly employ a DST approach to uncover insights on these structures' lifespan dynamics. Our approach can help enrich multiscale constitutive models, such as the promising H-model [17], which can incorporate the physics of grain loops and force chains to the extent that the *emergent* critical states can be reproduced. More broadly, a proper understanding of the birth-death dynamics of these structures benefits a gamut of applications where granular materials are subjected to shear, including the reduction of energy consumption and greenhouse gas emissions in processes such as comminution [18,19], the discovery and design of granular materials with enhanced properties, and geohazard forecasting [20], to name a few examples.

Prior studies have shown that the emergent mesostructures of force chains and grain loops are important building blocks for self-organization in two-dimensional (2D) and three-dimensional (3D) systems [5,6,21–24]. Prior work has highlighted that some statistical descriptors of the microstructure (e.g., fabric tensor, proportions of chained particles, proportions of the different categories of loops, etc.) reach constant values at the critical state [22,25–30]. Indeed, birth-death dynamics and related concepts such as "lifespan" are a promising way to think of the critical-state regime. Granular shear simulations and experiments, including those focusing on stick-slip dynamics, have shown that this regime is governed by the competing mechanisms of growth/birth versus collapse/death of force chains, and these events drive evolution towards, and during, stationary states of systems under shear [4,5,31–33]. Experimental evidence of detailed balance in sheared dense planar granular systems was recently reported by Sun *et al.* [34]. On the other hand, a DST analysis of DEM simulations for a 3D system in the critical-state regime uncovered bistable dynamics [5], which is governed by broken detailed balance and underlying conformational transitions having connections to the rattler dynamics reported by Wautier *et al.* [35]. Despite the significant attention paid to the topic, the following open questions that arise from all these studies remain: Why do granular systems evolve towards a stationary limiting state under continued shear? What mechanisms attract the system towards the critical state?

To quantify whether jamming dominates unjamming in evolving systems, the biology-inspired concepts of *lifespan* and *life expectancy* are particularly useful. Starting from a reference microstructure conformation, the lifespan of a mesostructure corresponds to the "time" it has continuously existed since its formation. Its life expectancy corresponds to the remaining time it will survive before disappearing. By comparing the distribution of lifespans and life expectancies, one can assess whether the birth rate of a particular class of mesostructure dominates its death rate. These concepts have been applied to granular materials; see, for instance, Refs. [30,36,37]. Indeed, these concepts enable the quantification of the renewal rate of the microstructure in both 2D and 3D conditions under an external forcing time parameter. Specifically, this quantification measures how fast the system is losing the memory of its past state under an external forcing. Consequently, the concepts of lifespan and life expectancy are particularly well adapted to treat granular materials from the perspective of dynamical systems with memory. In all these contexts, the time may correspond to physical time or any relevant forcing parameter, depending on the system of interest (for biaxial tests considered in the present study, the axial strain is the time parameter).

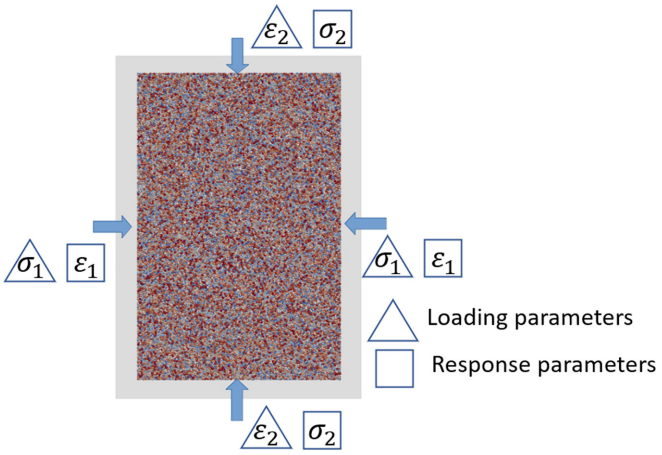

FIG. 1. Quasi-2D DEM sample for biaxial tests where loading parameters are ε_2 and σ_1. The direction 2 is always the vertical loading control direction at the representative element volume (REV) scale.

This paper is organized as follows. In Sec. II, the mechanical responses of granular samples under biaxial tests with DEM are analyzed. This is followed in Sec. III by a discussion on the critical state from a stationarity perspective. In this respect, the concepts of lifespan and life expectancy of mesostructures are applied to force chains and grain loops. Birth and death rates of chained particles and grain loops are analyzed in Sec. IV. The relations between microstructure dynamics and loading conditions are presented in Sec. V.

II. NUMERICAL SETUP

The discrete element method (DEM) proposed in Ref. [38] is widely used to simulate granular materials. The open-source DEM software YADE [39] is used in this study. The sample considered is a quasi-2D granular sample subjected to biaxial loadings under constant lateral pressure. The assembly consists of a single layer of 20 000 spherical particles contained in planar displacements within a 1-m-wide domain per 1.5 m high, as shown in Fig. 1. The particle radii are uniformly distributed with an average diameter $d_{50} = 0.008$ m and a size ratio $d_{\max}/d_{\min} = 2$. The contact law is described by a standard cohesionless elastofrictional law. The contact parameters between two grains contain normal and tangential linear springs of respective stiffness k_n and k_t, as well as a sliding limit characterized by a friction angle $\phi = 35^\circ$. $E = k_n/D_s$, given as 300 MPa, where $D_s = 2R_1R_2/(R_1 + R_2)$, and R_1, R_2 are the radii of particles.

TABLE I. Different initial confining levels.

Normalized initial confining pressure	A	B	C
P_0	1.3×10^{-4}	3.3×10^{-4}	1.3×10^{-3}

For sample preparation, two schemes can be used to obtain an isotropic compression of the sample in YADE DEM: the boundary moving scheme and the internal compacting scheme. In this study, particles are homothetically enlarged, at first, while keeping the boundary walls fixed to generate a preliminary sample with a certain level of confining pressure. Then, to get closer to an experimental setup, the sample undergoes an isotropic consolidation by imposing an equivalent incremental strain on the boundaries in the vertical and lateral directions up to a specific consolidation state. Three confining levels are considered, characterized by a dimensionless quantity P_0 representing the ratio $\frac{p_0}{E} = \frac{\sigma_1^0+\sigma_2^0}{2E}$ of the confining pressure over the stiffness, as shown in Table I. They are labeled as A, B, and C from the lowest to the highest. To prepare dense and loose samples, the contact friction angle is set to 2° and 35°, respectively, during the confining stage. Dense and loose samples are prepared and named as indicated in Table II. The initial void ratio e_0 and the ratio $\langle u_n \rangle / d_{50}$ of the average contact overlap and particle size of the samples prepared are presented. More details about sample preparation can be found in [8,25].

The stress and strain states are described using dimensionless quantities, the normalized deviatoric stress Q being defined as $Q = (\sigma_2 - \sigma_1)/E$, and the volumetric strain being defined as $\varepsilon_v = \varepsilon_1 + \varepsilon_2$, where σ_1 and σ_2 are the principal stresses, and ε_1 and ε_2 are the principal strains, as shown in Fig. 1. Axes 1 and 2 refer to lateral and vertical directions, respectively. Note that stresses σ_1 and σ_2 are computed in quasi-2D DEM simulations by introducing an out-of-plane dimension equal to the largest grain diameter ($d_{\max}$). If full 2D framework were preferred, the stress σ would be expressed in N/m and the dimensionless stresses P_0 and Q should be normalized by $E d_{\max}$ instead of E.

III. THE SO-CALLED CRITICAL STATE

In the literature, it is common to report fluctuations of the deviatoric stress and the volumetric strain around steady-state values rather than a smoothly constant evolution under biaxial loading. The evolution of micro and meso indices such as fabric tensor and ratio of loops population also exhibits fluctuations at the critical state. In this section, macroscopic stress and strain are considered in relation to the evolution of force chains and grain loop populations, respectively.

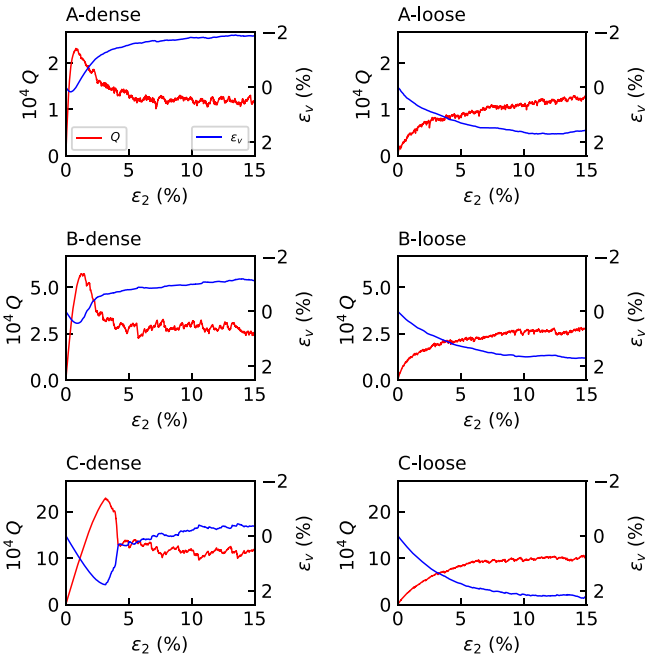

FIG. 2. Evolution of normalized deviatoric stress Q and volumetric strain ε_v with respect to the axial strain ε_2 along biaxial tests. Note that soil mechanics convention is adopted with positive compression and positive contraction.

A. Stress-strain analysis

Macroscopic responses of the tested samples are illustrated in Fig. 2, in which normalized deviatoric stress Q and volumetric strain ε_v evolve with respect to the axial strain ε_2. The figure shows typical stress and strain responses of dense and loose samples under the biaxial loadings.

In the dense cases, the normalized deviatoric stress Q increases at first and then decreases to a stationary value, while the sample contracts first and then dilates before reaching a steady state. With an increase in the confining pressure, there is an increase in the shear strength and a decrease in the dilation. On the other hand, the normalized deviatoric stress and volumetric strain in the loose samples evolve monotonously in the course of loading. It can be observed that, at the critical state, both the normalized deviatoric stress Q and the volumetric strain ε_v fluctuate around a constant value. Based on these mechanical responses, both the stationarity and the dynamical properties of the CS will be investigated in a micromechanical framework.

The incremental deviatoric strain distribution can be analyzed to characterize kinematic patterns, as introduced in the literature [30,40]. The maps are computed based on the interpolation of particle incremental displacements over a meshed sample [30,41]. When dense samples are considered, shear

TABLE II. Initial void ratios e_0 and average overlaps in prepared samples.

Sample	A-loose	B-loose	C-loose	A-dense	B-dense	C-dense
e_0	0.267	0.261	0.234	0.197	0.191	0.164
$\langle u_n \rangle / d_{50}$	9.2×10^{-4}	2.1×10^{-3}	7.6×10^{-3}	6.6×10^{-4}	1.6×10^{-3}	5.6×10^{-3}

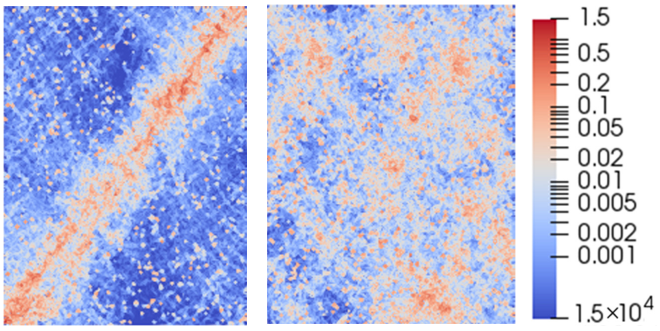

(a) (b)

FIG. 3. Incremental deviatoric strain (IDS) maps at the critical states, estimated for axial strain increments of 0.1%. Two samples are considered: (a) B-dense sample ($\varepsilon_2 = 6.1\%$) and (b) B-loose sample ($\varepsilon_2 = 8.02\%$).

bands may develop, traversing the whole sample as shown in Fig. 3. It is the spatial domain within shear bands for dense cases and the whole sample for loose cases that are considered in this study [26,30]. The spatial extension of the shear band was determined based on the method proposed in [41].

B. Force chains and normalized deviatoric stress

Force chains have attracted considerable interest due to their significant role in force transmissions in granular systems [23,42]. To consider force chains as individual mesostructures (and not as a network of strong contacts), the following three conditions were proposed by Peters *et al.* [43]:

(i) The number of contacting particles in a force chain is not less than 3.

(ii) The major principal stress in each particle belonging to a force chain is larger than the averaged assembly particle major principal stress.

(iii) The major principal stress direction is aligned with the contact direction with a deviation angle less than 45°.

In this paper, the particles belonging to force chains are called *chained particles*. The proportions of chained particles is given by $r_{\text{cha}} = N_{\text{cha}}/N_{\text{tot}}$, where N_{cha} and N_{tot} are the number of chained particles and the total number of particles within the investigated domain, respectively. The ratio within the shear band r^*_{cha} and the whole sample r_{cha} are compared in Fig. 4. It can be seen that the evolution with strain of both r^*_{cha} and r_{cha} tends to reach a constant value (with fluctuations) when the normalized deviatoric stress and the volumetric strain become constant at CS. r^*_{cha} is larger than r_{cha} after the generation of the shear band, with greater fluctuations. This may result in a stronger rearrangement of chained particles within the shear band. It is worth noting that the ratio of chained particles fluctuating around a mean constant value highlights the fact that important force chain reorganizations take place at the critical state.

C. Grain loops and volumetric strain

In a 2D granular material, grain loops, enclosed by contact branches, formed by tessellating the material area. It is usually categorized according to the edge number (from L_3 with three particles to L_{6p} for loops containing six or more particles), a factor that has a significant influence on the behavior of a loop, especially its deformability. The percentage of each category reaches a steady state that corresponds to the critical state regime at the sample scale [30]. It is worth noting that the reason for categorizing L_{6p} is that the percentage of L_{7p} (percentage of categories with a side number equal to or greater than 7) evolves in a similar way to that of L_6 [30]. In this section, we link the grain loop populations (L_3, L_4, L_5, L_{6p}) to the volumetric evolution along the biaxial test by introducing the volumetric strain of the different grain loops. The incremental strain tensor of each type of loop i can be expressed as follows:

$$d\bar{\bar{\varepsilon}}_{Li} = \frac{1}{|\Omega|}\sum_k |\Omega^k_{L_i}| d\bar{\bar{\varepsilon}}^k_{L_i}, \quad i \in (3, 4, 5, 6\text{p}), \tag{1}$$

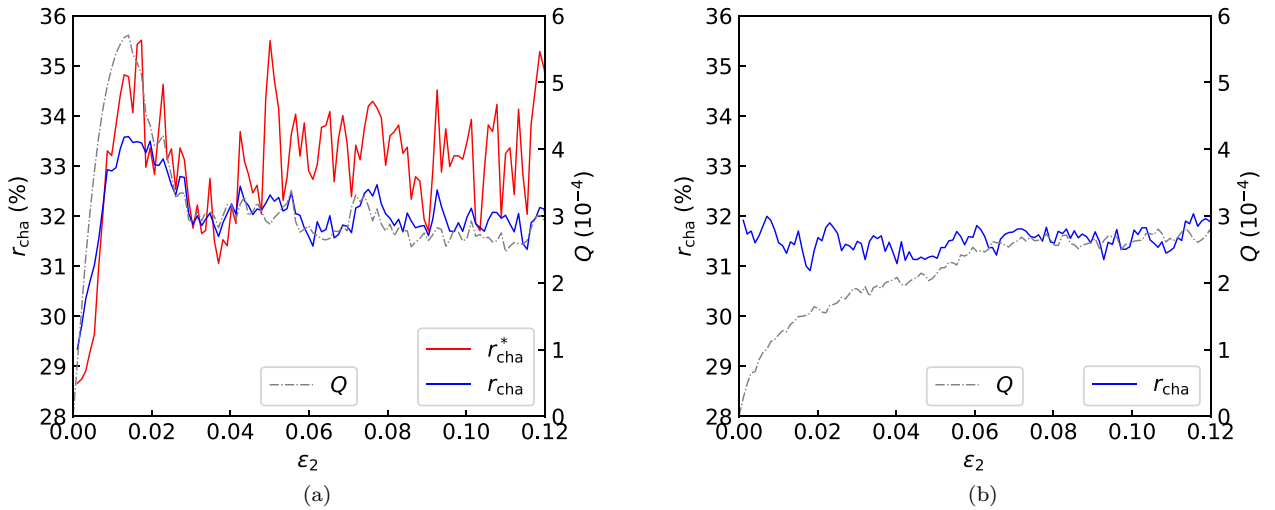

(a) (b)

FIG. 4. Proportions of chained particles. Two samples are considered: (a) B-dense sample and (b) B-loose sample. Note that r^*_{cha} represents the value when the spatial domain of a shear band is considered, and r_{cha} represents the value when the whole sample is considered. The normalized deviatoric stresses are recalled.

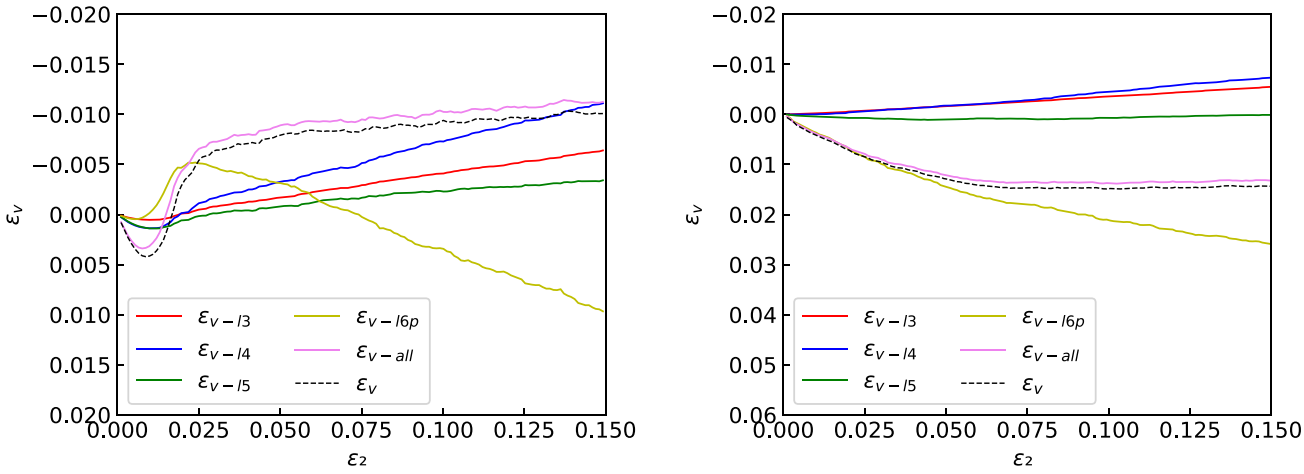

FIG. 5. Volumetric strain of different types of loops and the global assembly during the biaxial tests in B-dense sample (a) and B-loose sample (b).

where Ω is the volume of the global domain considered, and Ω^k_{Li} is the volume of a given loop k belonging to the category L_i. The incremental strain $d\bar{\bar{\varepsilon}}^k_{Li}$ of each loop k can be computed assuming a uniform deformation within that loop according to the strain definition proposed by Liu *et al.* [41].

The contribution of local incremental strains to the global incremental strain can be expressed by Eq. (2):

$$\langle d\bar{\bar{\varepsilon}}\rangle = \frac{1}{|\Omega|}\int_{\Omega} d\bar{\bar{\varepsilon}}dS = d\bar{\bar{\varepsilon}}_{L_3} + d\bar{\bar{\varepsilon}}_{L_4} + d\bar{\bar{\varepsilon}}_{L_5} + d\bar{\bar{\varepsilon}}_{L_{6p}}. \quad (2)$$

Figure 5 presents the volumetric strain of each category of loops and their integration during the biaxial loading as well as the evolution of the global volumetric strain. Figure 5 shows a good agreement between the macroscopically computed volumetric strain and the mesoscopically averaged one. Despite reaching a zero volume change on average, it can be seen that each loop category reaches constant dilative or contractive rates at the critical state. The dilatancy from L_3, L_4, and L_5, and the contractancy from L_{6p}, should be related to the inherent property of each loop: the grains belonging to L_i ($i \leqslant 5$) have limited space to move inward to induce contractancy, whereas L_{6p} loops have larger void space to move inward. As a result, the critical state can only be achieved from a collective process by loops transforming from one category to another.

IV. HIDDEN DYNAMICS AT THE CRITICAL STATE

As highlighted in the previous sections, the jamming and unjamming behavior at the critical state (CS) includes dynamic mechanisms at the mesoscale [4,31,33,34]. In this respect, the dynamical rates are investigated in this section through computing the lifespan and life expectancy of chained

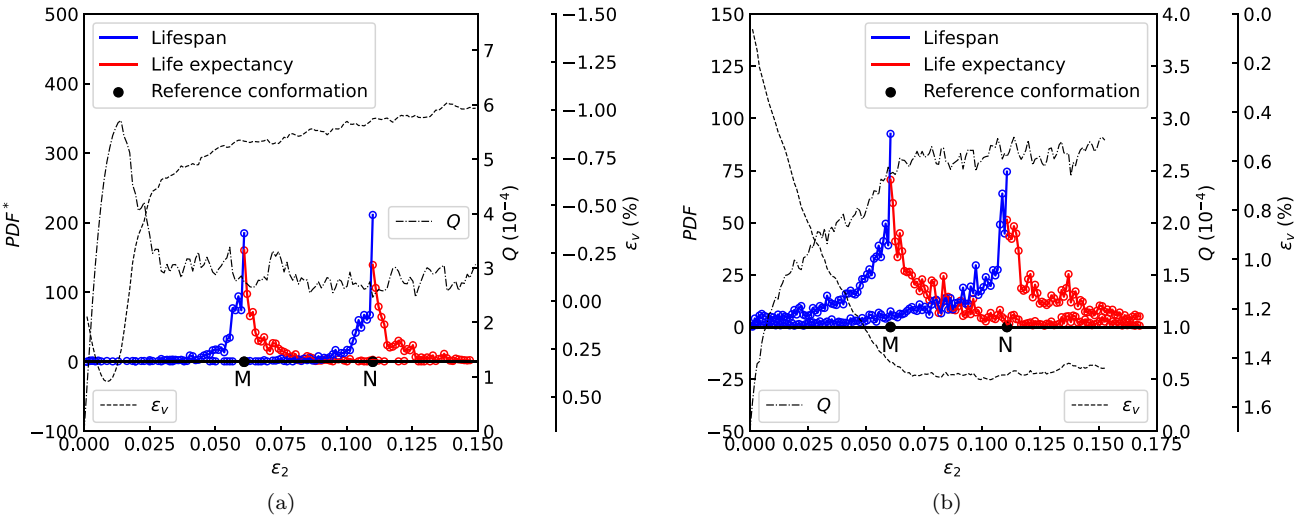

FIG. 6. Lifespan and life expectancy probability density functions (PDFs) of chained particles in two samples: (a) B-dense sample where only the spatial domain within the shear band is considered, and (b) B-loose sample with the whole domain considered. For each sample, two reference conformations belonging to the stationary regime are adopted, labeled as M and N. The normalized deviatoric stress curve (dot-dashed line) and the volumetric strain (dashed line) curves are recalled.

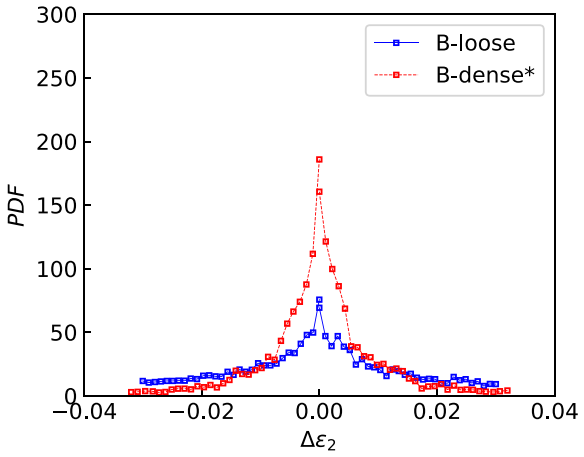

FIG. 7. The averaged PDFs of chained particles with respect to the incremental strain evolution ($\Delta\varepsilon_2$), over six microstructure conformations at different strain levels belonging to the critical regime ($\varepsilon_2 = 0.0610$, 0.0708, 0.0806, 0.0904, 0.1002, and 0.1100 for the B-dense sample, and $\varepsilon_2 = 0.0605$, 0.0708, 0.0802, 0.0906, 0.1005, and 0.1106 for the B-loose sample).

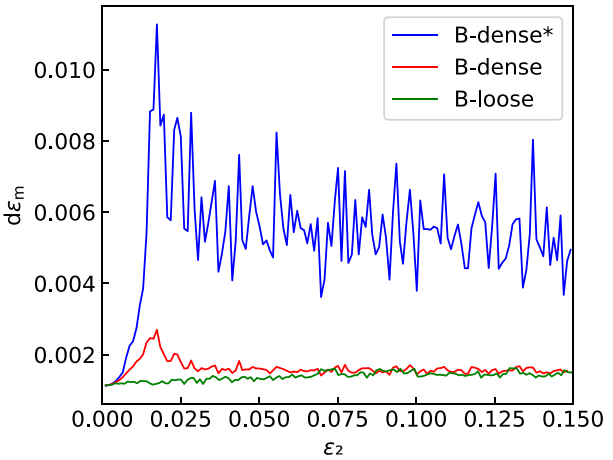

FIG. 8. The strain magnitudes within the shear band domain (B-dense*), the whole dense sample (B-dense), and the whole loose sample (B-loose). The strain magnitude ratio between B-dense* and B-dense is around 2.8.

particles and grain loops. The incremental evolutions of the sets of chained particles and grain loops are checked for small axial strain increments of $\delta\varepsilon_2 = 0.1\%$.

A. Generating and vanishing process of chained particles

All chained particles are tracked from birth, i.e., the first time they become part of a given force chain, to death, i.e., the first time they no longer belong to any force chain. This enables us to construct probability density functions (PDFs) for the lifespan and the life expectancy of chained particles at any time of the simulation. The lifespan and life expectancy PDFs are displayed in Fig. 6 for two arbitrary microstructure conformations (M and N) in the critical state regime. Because the sample is known to experience shear band localization (see Fig. 3), the analysis is restricted to particles belonging to the shear band in Fig. 6.

At the reference conformation M (N) in Fig. 6(a), the PDFs for the lifespan and life expectancy demonstrate the generating and vanishing processes of chained particles within the shear band domain. Few chained particles existing at M or N come from the initial conformation, which proves that the initial arrangement of particles has been erased when the sample reaches CS. The symmetric shape of the lifespan and life expectancy PDFs shows that the rearrangement of chained particles reaches an equilibrium at CS, which is expected for a stationary regime. More interestingly, the shape of the PDFs for the reference conformations M and N is almost the same. Force chains are always rearranging at the critical state, and the rate of renewal of the set of chained particles is constant. These features can be observed in B-loose with lower renewal rates from Fig. 6(b). The PDFs have been averaged to get rid of statistical noise coming from the finite size of the chained particle population at different strain levels belonging to the critical regime ($\varepsilon_2 = 0.0610$, 0.0708, 0.0806, 0.0904, 0.1002, and 0.1100 for the B-dense sample, and $\varepsilon_2 = 0.0605$, 0.0708, 0.0802, 0.0906, 0.1005, and 0.1106 for the B-loose sample). Since force chains have a limited life duration at the critical state, the six microstructure conformations can be considered as statistically independent (not correlated), which allows us to build a single PDF from the six data sets. The corresponding lifespan and life expectancy PDFs are presented in Fig. 7 with respect to the incremental evolution of the axial strain ($\Delta\varepsilon_2$). Thus, $\Delta\varepsilon_2$ at the current state is 0. $\Delta\varepsilon_2 > 0$ and $\Delta\varepsilon_2 < 0$ correspond to the lifespan and life expectancy of chained particles, respectively.

The renewal rate in dense and loose samples appears to be different at first glance, which would contradict the existence of a unique critical state regardless of the initial sample density. To find the origin of the apparent faster renewal rate within the shear band in the dense sample, it is meaningful to compare the incremental strain magnitude $d\varepsilon_m = \sqrt{d\varepsilon_1^2 + d\varepsilon_2^2}$ in the shear band domain for the dense sample to the incremental strain magnitude in the whole sample domain for the loose sample. Similar to the incremental strain of each type of loops computed in Sec. III C, the incremental strain within the shear band can be computed by averaging

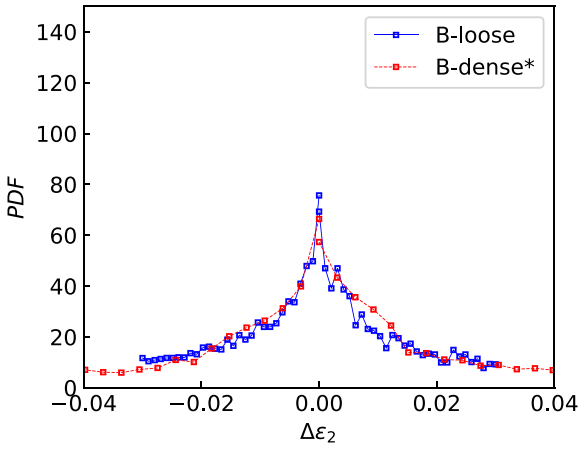

FIG. 9. PDFs for chained particles from the B-loose sample and from the B-dense sample stretched by the strain magnitude ratio 2.8.

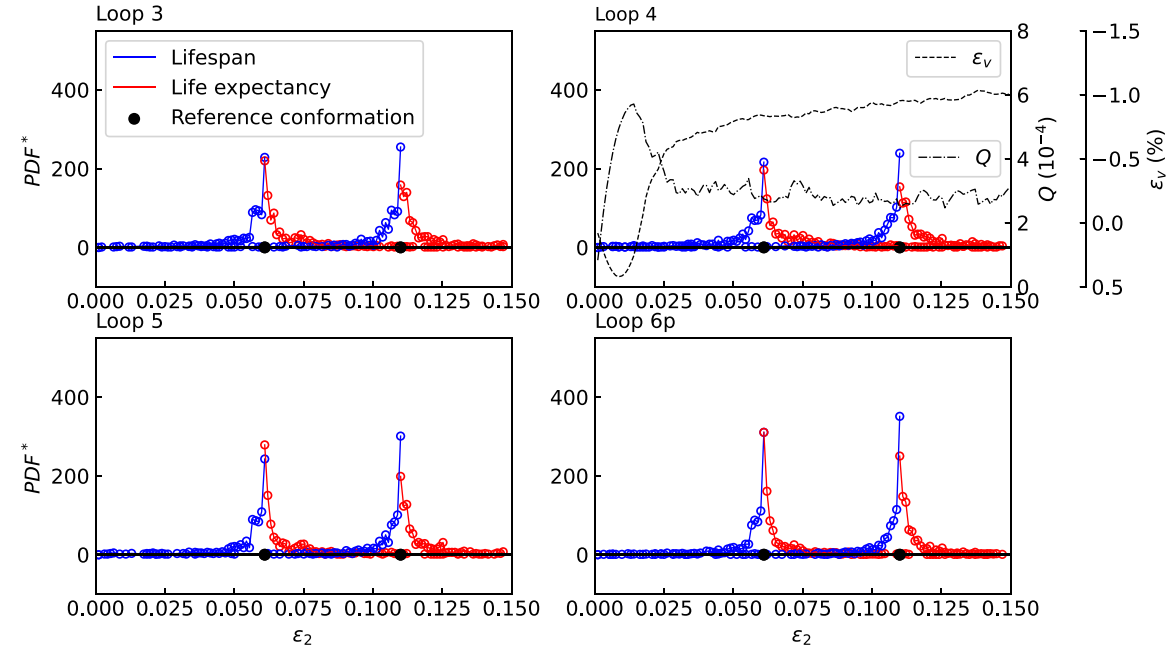

(a)

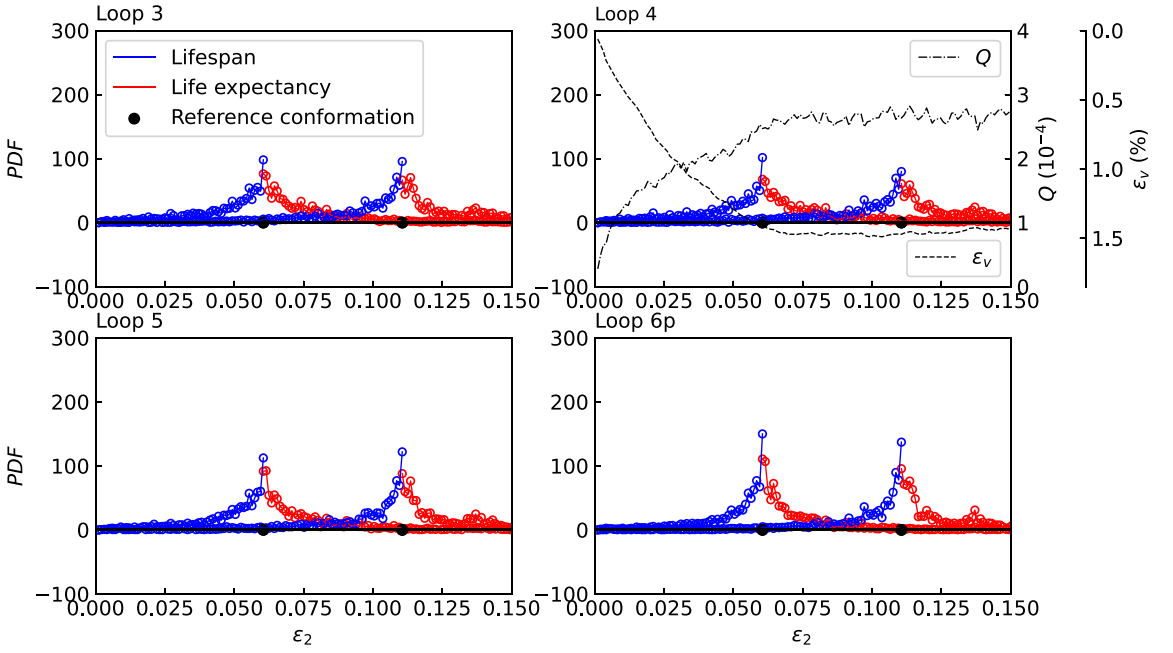

(b)

FIG. 10. Lifespan and life expectancy PDFs of grain loops in two samples with respect to the axial strain ε_2: (a) B-dense sample where only the spatial domain within the shear band is considered, and (b) B-loose sample with the whole domain considered. For each sample, two reference conformations belonging to the stationary regime are adopted. The normalized deviatoric stress curve (dot-dashed line) and the volumetric strain (dashed line) curves are recalled in the subfigure of Loop 4.

the incremental strains of loops within the shear band over the area of the shear band. When averaged over the whole sample domain, $d\varepsilon_m$ is the same in dense and loose samples at the critical state, as shown in Fig. 8. However, because of the strain localization in the dense sample, a larger $d\varepsilon_m^*$ develops within the shear band. The ratio between $\langle d\varepsilon_m^* \rangle$ and $\langle d\varepsilon_m \rangle$ at CS inside the shear band is around 2.8. In other words, an axial strain increment of 1% from the boundaries of the sample imposes a strain increment of 2.8% in the shear band domain because of strain localization. This means that the actual forcing parameter (the "time") inside the shear band is 2.8 times faster than for the whole sample. As a

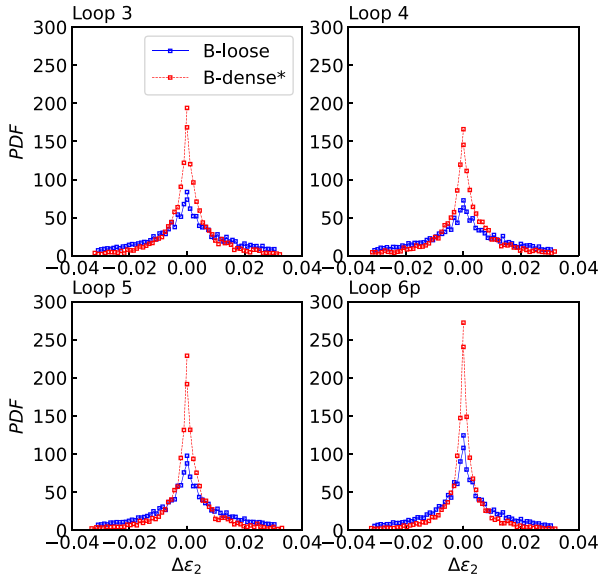

FIG. 11. The averaged PDFs of grain loops with respect to the incremental strain evolution ($\Delta\varepsilon_2$), over six microstructure conformations at different strain levels belonging to the critical regime ($\varepsilon_2 = 0.0610$, 0.0708, 0.0806, 0.0904, 0.1002, and 0.1100 for the B-dense sample, and $\varepsilon_2 = 0.0605$, 0.0708, 0.0802, 0.0906, 0.1005, and 0.1106 for the B-loose sample).

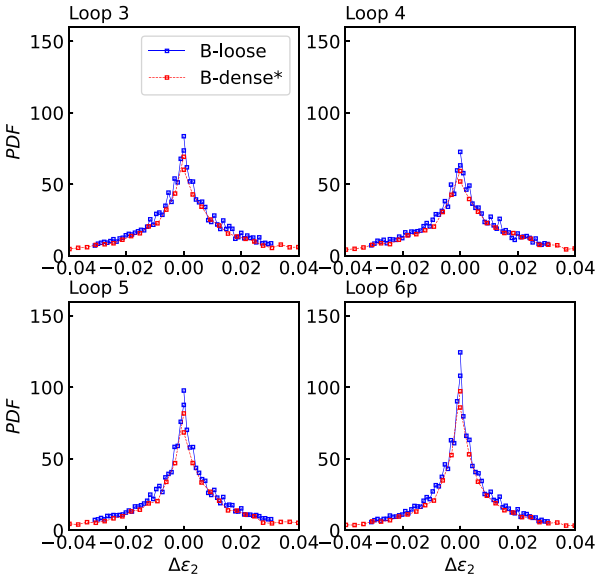

FIG. 12. PDFs for grain loops from the B-loose sample and from the B-dense sample stretched by the strain magnitude ratio 2.8.

result, the axial strain applied at sample scale is not the right forcing parameter in the dense case as the strain is 2.8 times more intense in the shear band domain. To account for this observation, we need to stretch the curves of B-dense* by the ratio 2.8 to make the lifespan and life expectancy PDF comparable between the dense and loose sample cases. Then, it can be observed in Fig. 9 that the PDF in dense and loose samples are coinciding. Similar results can be observed for different confining pressure levels, as shown in Figs. 20 and 21 in Appendix A. It can be concluded that the strain magnitude (observed in the homogeneous domain of the samples) is the major factor affecting the rate of rearrangement of chained particles. The fact that the PDFs coincide also demonstrates that the strain rate does not affect the reorganization process (at least for the order of magnitude considered). We can also conclude that the uniqueness of the critical state (i.e., regardless of the initial density, the statistical descriptors converge towards the same value in biaxial tests of similar confining pressure) that holds for statistical descriptors also holds for the underlying dynamical processes.

B. Generating and vanishing process of grain loops

To further understand the critical state dynamics, the generating and vanishing of grain loops are analyzed for loops composed of three, four, five, and six or more particles. Lifespan and life expectancy PDFs for grain loops are computed. Similar observations as reported in the previous subsections are visible in Figs. 10–12: (i) PDFs show symmetrical shapes at CS, which suggests that birth and death rates of grain loops are equal at CS; (ii) PDFs within the shear band from B-dense sample coincide with those obtained in the loose case after being stretched by the appropriate ratio of 2.8. These results extend the conclusion drawn by Zhu *et al.* [30], i.e., that the whole loose sample and the inner part of the shear band of the dense sample share the same statistical distribution of mesostructures once the critical state regime is reached. Based on Figs. 6–12, a novel way for understanding CS from the perspective of a mesoscale dynamics can be inferred: the critical state results from the generating and vanishing of mesoclusters until a dynamic equilibrium is reached under continuous shearing. Even though dynamic rearrangements permanently occur, at any time, the material admits the same fabric characterized by the fabric tensor, the distribution of loop orders, etc. The particle rearrangements at the critical state can be quantitatively characterized by the lifespan and life expectancy of force chains and grain loops. These observations still hold when other confining pressure levels (A and C) are considered, as shown in Appendix A.

V. MICROSTRUCTURE REORGANIZATION DYNAMICS UNDER DIFFERENT CONFINING PRESSURE LEVELS

In this section, the influence of the confining pressure on the dynamics in the three loose samples is analyzed. As shown in Figs. 13 and 14, the renewal rate decreases with the increase in the confining pressure. The increase in confining pressure helps the mesostructures live longer (with respect to the forcing parameter of the system, i.e., the incremental axial strain). This is consistent with the fact that larger confining pressure leads to larger elastic energy storage and larger overlap at contacts, which delays contact opening and contact sliding.

To quantify the rate of microstructure reorganization with respect to the axial strain, it is interesting to propose a fit for the PDFs presented so far. As a first simple guess, an exponential fit with one characteristic strain may been proposed as $\mathrm{PDF}(\Delta\varepsilon_2) = \frac{a}{\varepsilon_c} e^{-|\Delta\varepsilon_2|/\varepsilon_c}$. ε_c accounts for the typical size of the axial strain increment $\Delta\varepsilon_2$ needed to renew the whole mesostructures. The smaller ε_c is, the faster is the microstructure renewal under the external forcing $\Delta\varepsilon_2$. However, such a

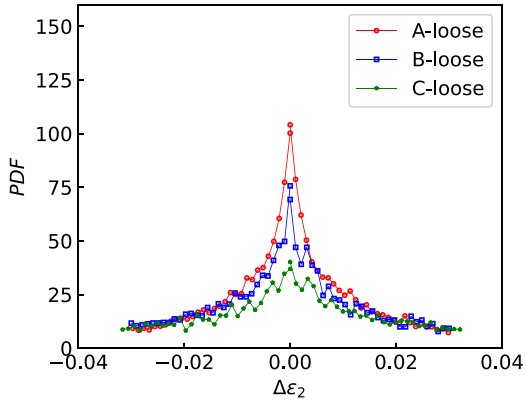

FIG. 13. Lifespan and life expectancy PDFs for chained particles under the different confining pressure levels with samples A-loose, B-loose, and C-loose considered.

fit cannot capture well the shape of the whole PDFs. Depending on ε_c, the fit is able to account either for the beginning or for the tail of the PDFs. This observation motivated the use of a double exponential fit in the following form:

$$\mathrm{PDF}(\Delta\varepsilon_2) = P_c \frac{1}{\varepsilon_{c1}} e^{-\frac{|\Delta\varepsilon_2|}{\varepsilon_{c1}}} + (1-P_c)\frac{1}{\varepsilon_{c2}} e^{-\frac{|\Delta\varepsilon_2|}{\varepsilon_{c2}}}, \qquad (3)$$

where ε_{c1} and ε_{c2} ($\varepsilon_{c1} < \varepsilon_{c2}$) correspond to two characteristic strains accounting for the dynamic evolution of the system. ε_{c1} and ε_{c2} account for the typical amplitude of the axial strain increments $\Delta\varepsilon_2$ needed to renew the mesostructures on the short term and long term, respectively. The characteristic probability $P_c \in [0, 1]$ can show the relative contribution of the short- and long-term mechanisms. When $P_c < 0.5$, it is the long-term mechanism that dominates; the short-term mechanism will be more important when $P_c > 0.5$; the two

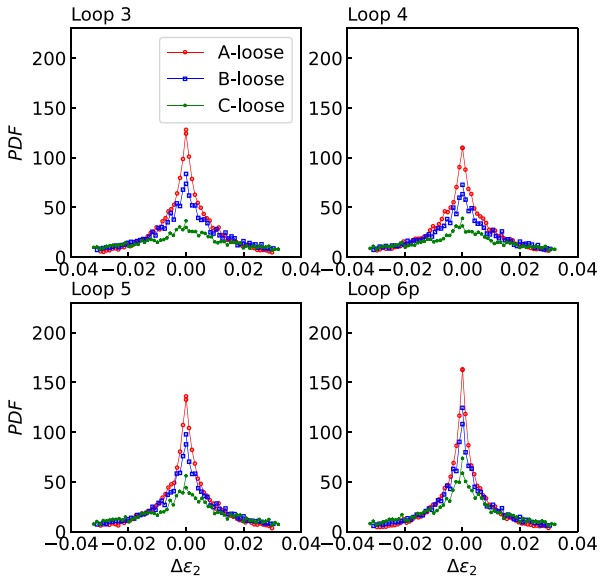

FIG. 14. Lifespan and life expectancy PDFs for grain loops with respect to the incremental strain evolution ($\Delta\varepsilon_2$) under the different confining pressure levels with samples A-loose, B-loose, and C-loose considered.

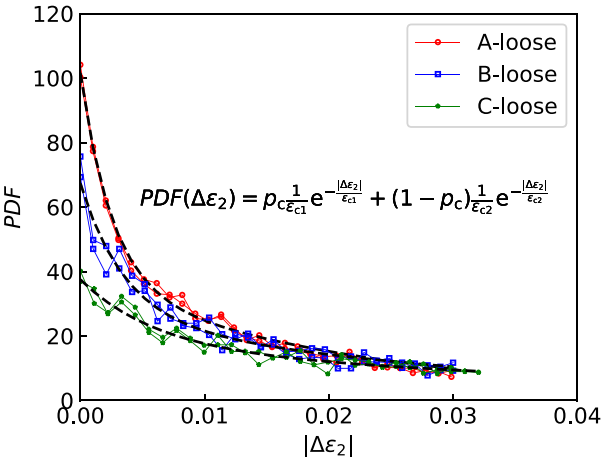

FIG. 15. Double-exponential fits given for the chained particle PDFs with respect to the absolute value of incremental evolution $|\Delta\varepsilon_2|$ under the different confining pressure levels.

mechanisms are evenly matched when $P_c = 0.5$. Figures 15 and 16 show that a double exponential fit is able to account for the shape of all the lifespan and life expectancy PDFs. The values of ε_{c1} and ε_{c2} for different confining pressure levels are presented in Table III and shown in Fig. 17 with respect to the normalized critical mean stress $P = \frac{\sigma_1+\sigma_2}{2E}$.

As shown in Table III and Fig. 17, large loops (L_5 and L_{6p}) live shorter (faster reorganization) than small loops (L_3 and L_4) and force chains. It is consistent with the assumption that loops connected to force chains open prior to force chain bending [44]. When it comes to the effect of confining pressures, the renewal rate of mesostructures which can be characterized by $\frac{1}{\varepsilon_{c1}}$ and $\frac{1}{\varepsilon_{c2}}$ decreases with the increase in

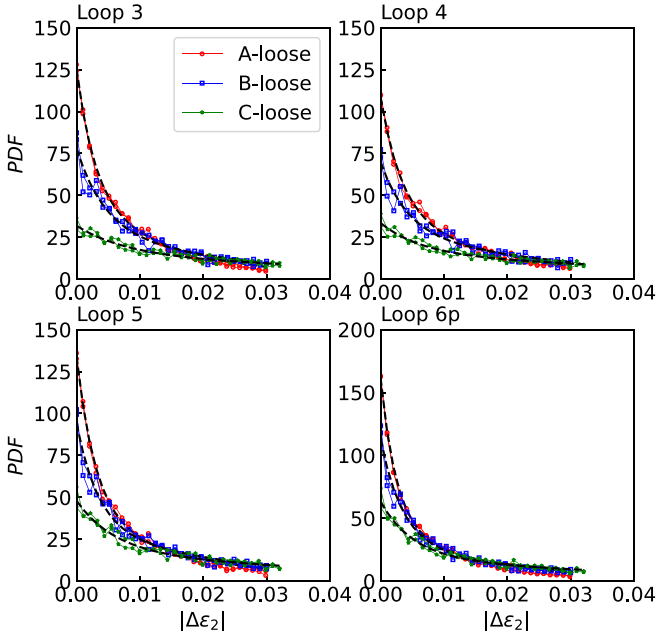

FIG. 16. Double-exponential fits given for the loop PDFs with respect to the absolute value of incremental evolution $|\Delta\varepsilon_2|$ under the different confining pressure levels.

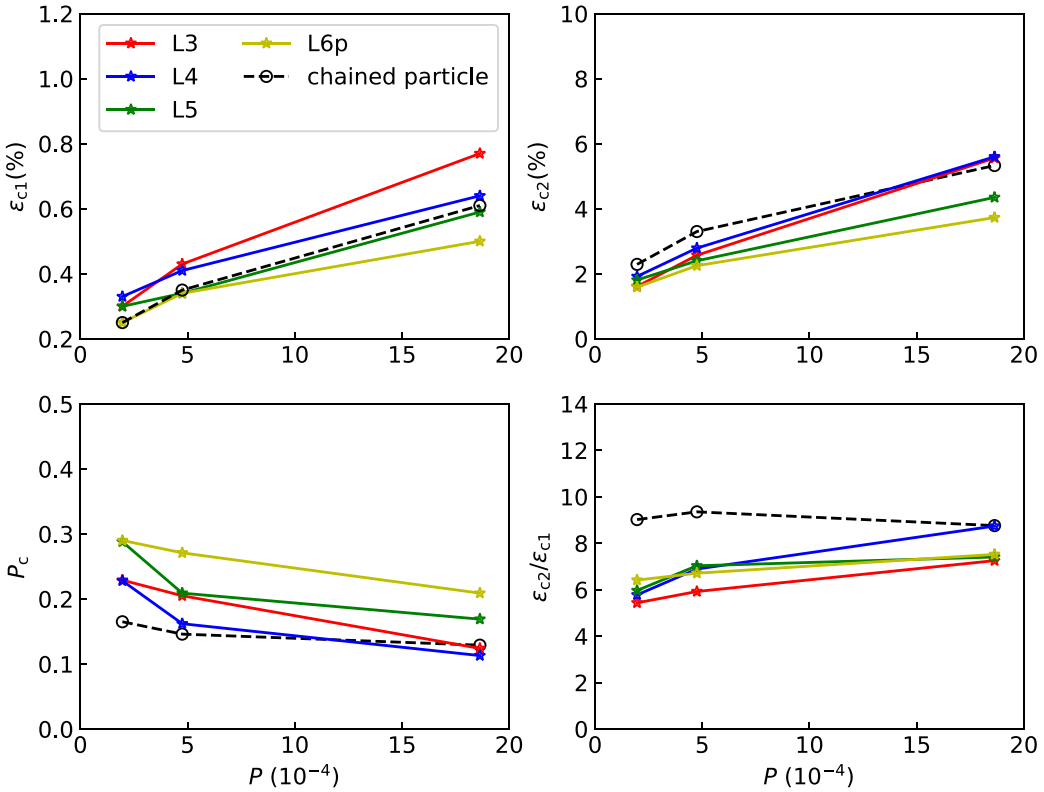

FIG. 17. Two characteristic strains (ε_{c1} and ε_{c2}), the characteristic probability (P_c), and the ratio $\frac{\varepsilon_{c1}}{\varepsilon_{c1}}$ with respect to the normalized mean stress (P) at the critical state. The normalized critical mean stress under the different confining pressure levels (A, B, and C) is 1.97×10^{-4}, 4.77×10^{-4}, and 18.63×10^{-4}, respectively.

the confining pressure. This effect differs according to the type of mesostructures. L_3 and L_4 seem to be more sensitive to the confining pressures, especially in the long-term mechanism, which could be due to the fact that these small, less compressible loops can store larger (stabilizing) elastic energy before breaking. On the other hand, large loops (L_5 and L_{6p}) are more compressible, and therefore less sensitive to confining pressure, as the increase in p does not have as much stabilization effect as for smaller loops. As for chained particles, even though force chains can share particles with large loops, their stability (and thus lifespan) is strongly dependent on the existence of small order loops around them. Thus, the effect of confining pressure on force chain lifespan stems from the different responses of loops under the confining pressure according to their category (small versus large ones), which may explain why the slope of the ε_{c1} and ε_{c2} for chained particles is smaller than that for small loops but larger than that for large loops. In addition, the long-term mechanism has an increasingly dominant effect, since P_c, always being less than 0.5, decreases with the growth of critical pressures. The form of the proposed fit may appear arbitrary at first glance, but a double exponential PDF is the signature of the existence of two mechanisms responsible for microstructure reorganization acting over two different "time" scales. A first mechanism provokes microstructure reorganizations over small axial strain scales of typical magnitude ε_{c1}, while a second mechanism induces microstructure reorganizations over much larger axial strain scales of typical magnitude ε_{c2}. The existence of two reorganization mechanisms is indeed consistent with the visualization of the incremental deviatoric strain map in Fig. 3 for the loose sample. The map is far from being homogeneous over the whole sample domain, and zones with large increments of deviatoric strain are visible (in the form of red zones in Fig. 3). Contrary to shear bands, these zones do not persist when the axial strain increases as shown. Indeed, these zones may be seen as shear transformation zones (STZs) [45], and they are characterized by the recent concept of shear chain [46]. As a result, we conjecture that ε_{c1} relates

TABLE III. The fitting parameters for different confining pressure levels.

Sample	Parameters	Chained particles	L_3	L_4	L_5	L_{6p}
A-loose	ε_{c1}	0.25%	0.30%	0.33%	0.30%	0.25%
	ε_{c2}	2.29%	1.61%	1.92%	1.81%	1.59%
	P_c	0.165	0.229	0.228	0.288	0.290
	$\varepsilon_{c1}/\varepsilon_{c2}$	9.02	5.44	5.78	5.97	6.41
B-loose	ε_{c1}	0.35%	0.43%	0.41%	0.34%	0.34%
	ε_{c2}	3.30%	2.57%	2.79%	2.40%	2.25%
	P_c	0.146	0.205	0.162	0.209	0.271
	$\varepsilon_{c1}/\varepsilon_{c2}$	9.35	5.92	6.89	7.03	6.71
C-loose	ε_{c1}	0.61%	0.77%	0.64%	0.59%	0.50%
	ε_{c2}	5.33%	5.56%	5.60%	4.35%	3.73%
	P_c	0.129	0.124	0.113	0.169	0.209
	$\varepsilon_{c1}/\varepsilon_{c2}$	8.76	7.25	8.74	7.41	7.52

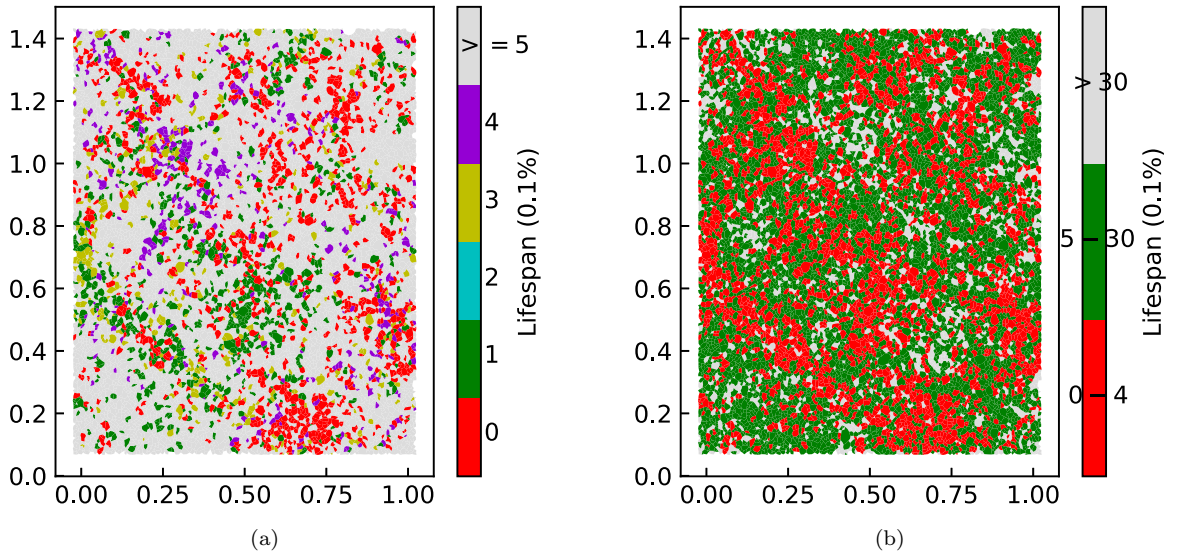

(a) (b)

FIG. 18. Color maps of the lifespan of grain loops for the reference axial strain $\varepsilon_2 = 8.02\%$. Two thresholds are considered corresponding to the two characteristic strains: (a) 0.4% and (b) 3%.

to the axial strain needed for a shear transition zone to develop, while $\varepsilon_{c2} > \varepsilon_{c1}$ corresponds to the axial strain needed to develop shear transition zones everywhere in the sample domain. This conjecture can be initially verified by the color maps of lifespan and life expectancy of loops in the sample B-loose, as shown in Figs. 18 and 19, respectively.

The short and long thresholds are set to $4\delta\varepsilon_2$ and $30\delta\varepsilon_2$, respectively. In Fig. 18(a), red loops are newly generated at the current conformation. The loops that have lived longer than $4\delta\varepsilon_2$ are filled in gray. Figure 18(a) shows that the microstructure is experiencing a series of localized reorganizations (visible as clusters of loops of the same colors) affecting a limited proportion of the sample domain. In the long term, these series of reorganizations will affect the whole sample domain as shown in Fig. 18(b), where loops that have existed not less than $30\delta\varepsilon_2$ are very limited. In Fig. 19(a), gray loops are those that will live longer than four steps. It can also be observed in Fig. 19(b) that beyond the long threshold, only a small part of the loops will still be alive.

VI. CONCLUSION

We revisit the critical state, which has been emphasized as a stationary state in geomechanics, and we characterize it using a dynamical system analysis of grain structures and their rearrangements. We have shown that the critical state results from a balance between the birth and death of meso-clusters. We have established that force chains and grain loops have a regular, short life duration (0.4–3% compared to the whole 15% loading) at the critical state, corresponding to a

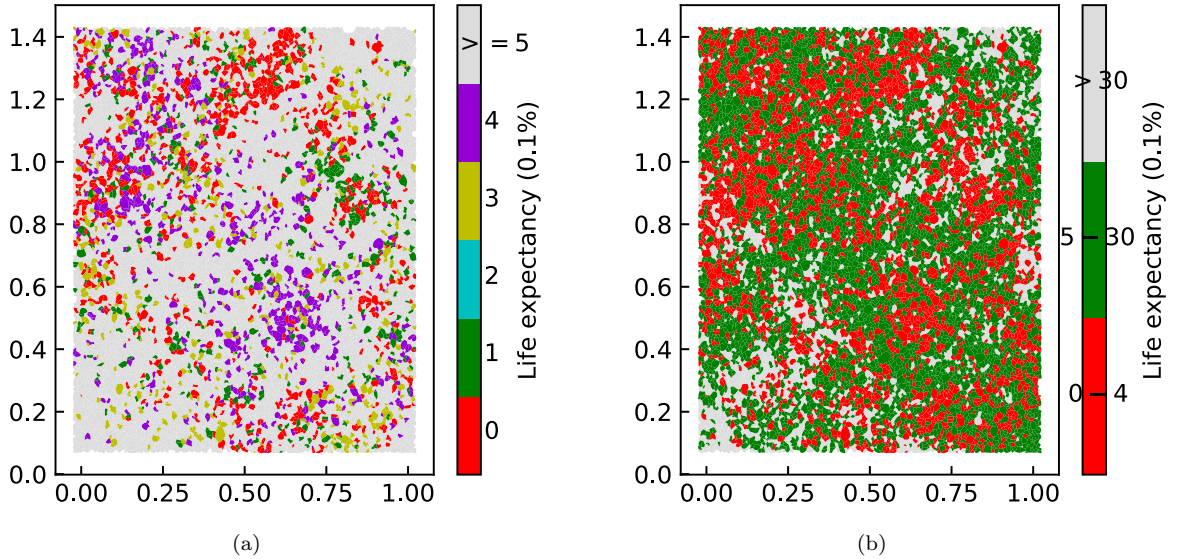

(a) (b)

FIG. 19. Color maps of the life expectancy of grain loops for the reference axial strain $\varepsilon_2 = 8.02\%$. Two thresholds are considered corresponding to the two characteristic strains: (a) 0.4% and (b) 3%.

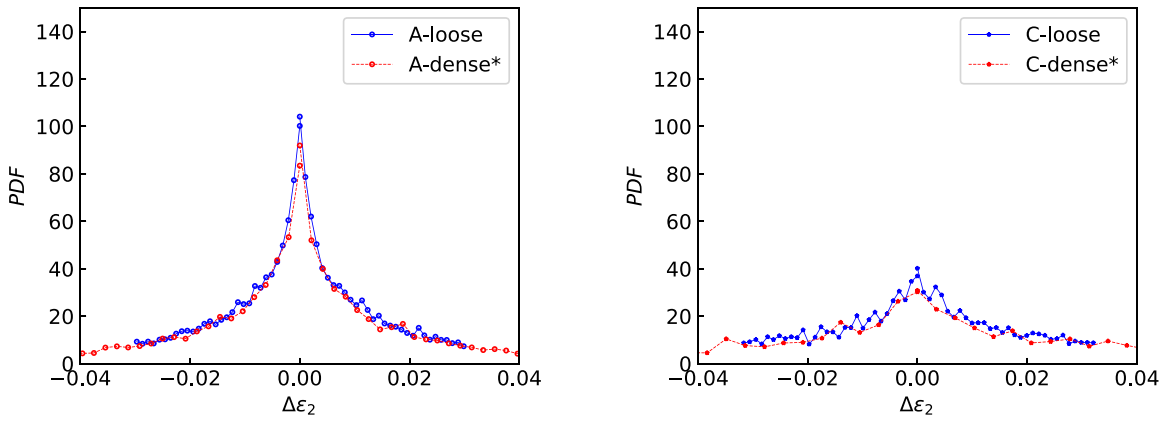

(a) (b)

FIG. 20. PDFs for chained particles under two confining pressure levels: (a) A, PDFs from the A-dense are stretched by strain magnitude ratio 1.9; (b) C, the C-dense stretched by 3.2.

rapid fading of the material memory along its loading history. The critical state "forgot" not just the initial microstructure conformation but its recent past in a sample under continuous shearing. We have shown that the uniqueness of the critical state that holds for statistical descriptors also holds for the underlying dynamical processes. By fitting the data, we have shown that force chains and loops of different sizes have different lifespan and life expectancy, which increases with the normalized mean stress level. Larger loops have a shorter life due to their deformability, and the force chain life duration is similar to the life duration of small order loops, which is consistent with the known relationship between force chains and their small order supporting loops. Moreover, the microstructure reorganization has been proved to rely on two mechanisms that act over very different axial strain increments. A local mechanism related to sheared mesostructures provokes a rapid (i.e., for small axial strain increments) reorganization of the microstructure, while the characteristic strain that relates to the nucleation of new sheared mesostructures accounts for the reorganizations over larger axial strain increments. The recent concept of shear chain [46] may also shed further light on the elastic and plastic mechanisms responsible for the observed dynamics of the critical state. The velocity of strain waves in the sample merits future investigation, since the dynamic load transfer characteristics can also be interpreted within the context of wave propagation theory [47]. In particular, such work may help elucidate whether the unjammed microstructure retains a partial memory of its previous jammed state. The findings presented in this paper also provide further clues on how to explicitly incorporate CS features in micromechanical constitutive models, as well as to limit the number of different loading paths needed to construct the database in data-driven models because of the limited hysteresis effect. In relation to a particular micromechanical model, it would be possible to consider the rearrangement of the hexagonal loop mesostructures relied on within the H-model [17,48] to achieve a better description of the critical state, based on the renewal rate of mesostructures as quantified in this study. Although the present study deals with the critical state dynamics in granular materials, the concepts and methodology proposed here are generic and may be applied to uncover the hidden dynamics of many other complex systems.

ACKNOWLEDGMENTS

The authors express their sincere thanks to the IRN (International Research Network) GeoMech for promoting positive and convivial interactions and discussions among researchers. The support from CSC (China Scholarship Council) under Grant CSC No. 201801810030 and from the BRGM (French Geological Survey), France under Contract No. RP19DRP023 is gratefully acknowledged. The constructive comments by the reviewers are appreciated.

APPENDIX A: COMPLEMENTARY RESULTS ON CRITICAL STATE DYNAMICS

In addition to the results presented in the main part of the paper, Figs. 20 and 21 provide complementary results on (a) the detailed balance achieved at the critical state for varying confining pressure levels, and (b) the uniqueness of the PDF for lifespan and life expectancy in dense and loose samples provided the strain rate is rescaled in the dense case to account for strain localization.

APPENDIX B: GLOSSARY OF TERMS

In this Appendix, we provide definitions of the main terms used in this paper.

1. Lifespan and life expectancy

The lifespan of a mesostructure corresponds to the time it has continuously existed since its appearance, where time here is characterized by axial strain increments. Life expectancy corresponds to the remaining time the mesostructure survives before its disappearance. These concepts can be applied for mesostructures in both 2D and 3D cases.

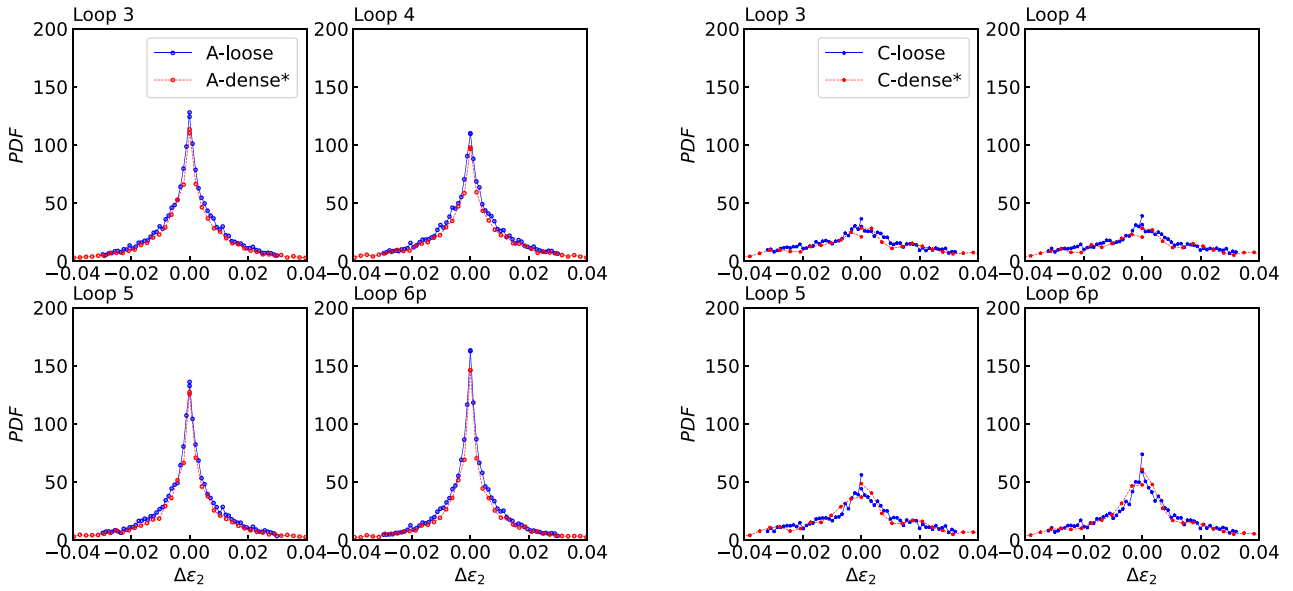

(a) (b)

FIG. 21. PDFs for grain loops under two confining pressure levels: (a) A, PDFs from the A-dense are stretched by strain magnitude ratio 1.9; (b) C, the C-dense stretched by 3.2.

2. Grain loop

Grain loop, enclosed by contact branches, is formed by tessellating the material area in 2D granular materials. The term "grain loop" refers here to the concept of minimal cycles in graph theory. In 2D, grain loops enclose polygons that form a partition of the sample domain that is able to characterize the dilatant/contractive behavior of granular materials. Even if cycles exist in 3D, the bijective link with a partition of the material volume is lost, which restricts the definition of grain loops to 2D conditions. Current work is aimed at generalizing the definition of such mesostructures to both 2D and 3D conditions [49]. The difference from the minimal cycles in the literature [22] is that grain loops have the connotation of volume.

3. Force chain

A force chain consists of a set of particles within a compressed granular material that are held together and jammed into place by a network of mutual compressive forces [43]. To consider force chains as individual mesostructures (and not as a network of strong contacts [42]), the definition used in the paper includes three thresholds, as detailed in Sec. III B.

4. Critical state

A critical state in soil mechanics is a macroscopic state where the stress and porosity of a material remain constant under continuous shearing. In standard soil mechanics, a set of critical state points forms a line in the (e, p, q) space (e being the void ratio, p the mean stress, and q the deviatoric stress), known as the critical state line. From a statistical physics viewpoint, the critical state is a steady state that relies on equivalent microstructure conformations. Macroscopic variables (such as stress or void ratio) computed on these different microstructure conformations are equal.

5. Conformation

Conformation is used to describe any spatial arrangement of grains in a given structure, while a conformational transition is a change in the conformation [4].

[1] M. R. Gardner and W. R. Ashby, Connectance of large dynamic (cybernetic) systems: Critical values for stability, Nature (London) **228**, 784 (1970).

[2] R. M. May, Will a large complex system be stable? Nature **238**, 413 (1972).

[3] L. Papadopoulos, M. A. Porter, K. E. Daniels, and D. S. Bassett, Network analysis of particles and grains, J. Complex Netw. **6**, 485 (2018).

[4] A. Tordesillas, D. M. Walker, G. Froyland, J. Zhang, and R. P. Behringer, Transition dynamics and magic-number-like behavior of frictional granular clusters, Phys. Rev. E **86**, 011306 (2012).

[5] S. Pucilowski and A. Tordesillas, Rattler wedging and force chain buckling: Metastable attractor dynamics of local grain rearrangements underlie globally bistable shear banding regime, Granular Matter **22**, 18 (2020).

[6] D. M. Walker, A. Tordesillas, N. Brodu, J. A. Dijksman, R. P. Behringer, and G. Froyland, Self-assembly in a near-frictionless granular material: Conformational structures and transitions in

uniaxial cyclic compression of hydrogel spheres, Soft matter **11**, 2157 (2015).

[7] R. P. Behringer and B. Chakraborty, The physics of jamming for granular materials: A review, Rep. Prog. Phys. **82**, 012601 (2018).

[8] J. Liu, A. Wautier, S. Bonelli, F. Nicot, and F. Darve, Macroscopic softening in granular materials from a mesoscale perspective, Int. J. Solids Struct. **193**, 222 (2020).

[9] T. Matsushima and R. Blumenfeld, Universal structural characteristics of Planar Granular Packs, Phys. Rev. Lett. **112**, 098003 (2014).

[10] R. Milo, S. Shen-Orr, S. Itzkovitz, N. Kashtan, D. Chklovskii, and U. Alon, Network motifs: Simple building blocks of complex networks, Science **298**, 824 (2002).

[11] A. Tordesillas, Force chain buckling, unjamming transitions and shear banding in dense granular assemblies, Philos. Mag. **87**, 4987 (2007).

[12] D. M. Walker, A. Tordesillas, M. Small, R. P. Behringer, and C. K. Tse, A complex systems analysis of stick-slip dynamics of a laboratory fault, Chaos **24**, 013132 (2014).

[13] K. H. Roscoe, A. Schofield, and A. P. Wroth, On the yielding of soils, Geotechnique **8**, 22 (1958).

[14] K. Been, M. Jefferies, and J. Hachey, The critical state of sands, Geotechnique **41**, 365 (1991).

[15] A. Casagrande, Characteristics of cohesionless soils affecting the stability of slopes and earth fills, J. Boston Soc. Civil Eng. **23**, 13 (1936).

[16] J. W. Rocks, A. J. Liu, and E. Katifori, Hidden Topological Structure of Flow Network Functionality, Phys. Rev. Lett. **126**, 028102 (2021).

[17] F. Nicot and F. Darve, The h-microdirectional model: Accounting for a mesoscopic scale, Mech. Mater. **43**, 918 (2011).

[18] D. M. Walker, A. Tordesillas, I. Einav, and M. Small, Complex networks in confined comminution, Phys. Rev. E **84**, 021301 (2011).

[19] O. Ben-Nun, I. Einav, and A. Tordesillas, Force Attractor in Confined Comminution of Granular Materials, Phys. Rev. Lett. **104**, 108001 (2010).

[20] A. Tordesillas, S. Kahagalage, L. Campbell, P. Bellett, E. Intrieri, and R. Batterham, Spatiotemporal slope stability analytics for failure estimation (SSSAFE): linking radar data to the fundamental dynamics of granular failure, Sci. Rep. **11**, 9729 (2021).

[21] S. Antony, Link between single-particle properties and macroscopic properties in particulate assemblies: Role of structures within structures, Philos. Trans. R. Soc., A **365**, 2879 (2007).

[22] A. Tordesillas, D. M. Walker, and Q. Lin, Force cycles and force chains, Phys. Rev. E **81**, 011302 (2010).

[23] A. Drescher and G. D. J. De Jong, Photoelastic verification of a mechanical model for the flow of a granular material, J. Mech. Phys. Solids **20**, 337 (1972).

[24] T. Majmudar, M. Sperl, S. Luding, and R. P. Behringer, Jamming Transition in Granular Systems, Phys. Rev. Lett. **98**, 058001 (2007).

[25] N. Deng, A. Wautier, Y. Thiery, Z.-Y. Yin, P.-Y. Hicher, and F. Nicot, On the attraction power of critical state in granular materials, J. Mech. Phys. Solids **149**, 104300 (2021).

[26] P. Fu and Y. F. Dafalias, Fabric evolution within shear bands of granular materials and its relation to critical state theory, Int. J. Numer. Anal. Methods Geomech. **35**, 1918 (2011).

[27] N. P. Kruyt and L. Rothenburg, On micromechanical characteristics of the critical state of two-dimensional granular materials, Acta Mech. **225**, 2301 (2014).

[28] L. Rothenburg and N. P. Kruyt, Critical state and evolution of coordination number in simulated granular materials, Int. J. Solids Struct. **41**, 5763 (2004).

[29] R. Wang, Y. F. Dafalias, P. Fu, and J.-M. Zhang, Fabric evolution and dilatancy within anisotropic critical state theory guided and validated by dem, Int. J. Solids Struct. **188**, 210 (2020).

[30] H. Zhu, H. N. Nguyen, F. Nicot, and F. Darve, On a common critical state in localized and diffuse failure modes, J. Mech. Phys. Solids **95**, 112 (2016).

[31] M. R. Kuhn, The critical state of granular media: Convergence, stationarity and disorder, Géotechnique **66**, 902 (2016).

[32] M. R. Kuhn, Maximum disorder model for dense steady-state flow of granular materials, Mech. Mater. **93**, 63 (2016).

[33] A. Rechenmacher, S. Abedi, and O. Chupin, Evolution of force chains in shear bands in sands, Géotechnique **60**, 343 (2010).

[34] X. Sun, Y. Wang, Y. Wang, R. Blumenfeld, and J. Zhang, Experimental evidence of detailed balance in granular systems, arXiv:2105.01355.

[35] A. Wautier, S. Bonelli, and F. Nicot, Rattlers' contribution to granular plasticity and mechanical stability, Int. J. Plasticity **112**, 172 (2019).

[36] N. Deng, A. Wautier, Y. Thiery, Z.-Y. Yin, P.-Y. Hicher, and F. Nicot, Dynamic view of critical state regime in granular materials: A mesoscale perspective, EPJ Web Conf. **249**, 11011 (2021).

[37] A. Wautier, S. Bonelli, and F. Nicot, Flow impact on granular force chains and induced instability, Phys. Rev. E **98**, 042909 (2018).

[38] P. A. Cundall and O. D. Strack, A discrete numerical model for granular assemblies, Geotechnique **29**, 47 (1979).

[39] V. Šmilauer, E. Catalano, B. Chareyre, S. Dorofeenko, J. Duriez, A. Gladky, J. Kozicki, C. Modenese, L. Scholtès, L. Sibille, *et al.*, Yade documentation 2nd ed. the yade project (2015), http://yade-dem.org/doc/.

[40] C. O'Sullivan, J. D. Bray, and S. Li, A new approach for calculating strain for particulate media, Int. J. Numer. Anal. Methods Geomech. **27**, 859 (2003).

[41] J. Liu, F. Nicot, and W. Zhou, Sustainability of internal structures during shear band forming in 2*d* granular materials, Powder Technol. **338**, 458 (2018).

[42] F. Radjai, M. Jean, J.-J. Moreau, and S. Roux, Force Distributions in Dense Two-Dimensional Granular Systems, Phys. Rev. Lett. **77**, 274 (1996).

[43] J. Peters, M. Muthuswamy, J. Wibowo, and A. Tordesillas, Characterization of force chains in granular material, Phys. Rev. E **72**, 041307 (2005).

[44] A. Wautier, S. Bonelli, and F. Nicot, Micro-inertia origin of instabilities in granular materials, Int. J. Numer. Anal. Methods Geomech. **42**, 1037 (2018).

[45] P. Schall, D. A. Weitz, and F. Spaepen, Structural rearrangements that govern flow in colloidal glasses, Science **318**, 1895 (2007).

[46] F. Darve, F. Nicot, A. Wautier, and J. Liu, Slip lines versus shear bands: Two competing localization modes, Mech. Res. Commun. **114**, 103603 (2021).

[47] M. H. Sadd, G. Adhikari, and F. Cardoso, Dem simulation of wave propagation in granular materials, Powder Technol. **109**, 222 (2000).

[48] A. Wautier, G. Veylon, M. Miot, M. Pouragha, F. Nicot, R. Wan, and F. Darve, Multiscale modelling of granular materials in boundary value problems accounting for mesoscale mechanisms, Comput. Geotech. **134**, 104143 (2021).

[49] J. Chueire, A. Wautier, F. Nicot, and A. Daouadji, On the extension of the grain loop concept from 2D to 3D granular assemblies (unpublished).